Testing the validity of small angle and adsorption-based characterization techniques by atomic-scale simulation

R. J. M. Pellenq[*] and B. Coasne[**]

[*]Centre de Recherche sur la Matiere Condensee et Nanosciences, CNRS, Campus de Luminy, 13288 Marseille cedex 09, France, pellenq@crmcn.univ-mrs.fr
[**]Laboratoire de Physicochimie de la Matière Condensée, CNRS et Université Montpellier 2, 30 place Eugène Bataillon, 34095 Montpellier Cedex 05, France, bcoasne@lpmc.univ-montp2.fr

ABSTRACT

This work aims at testing small angle and adsorption/desorption-based characterization techniques that are routinely used for nanoporous material characterization (specific surface and pore size distribution measurements). For that purpose, we report Grand Canonical Monte Carlo results of Ar adsorption at 77 K in various silica nanopores including cylindrical, ellipsoidal, and constricted pores and a Vycor-like matrix. Both the morphological and topological disorders are shown to significantly affect the adsorption and capillary condensation of fluids and, therefore, the data estimated from the characterization techniques.

Keywords: nanopores, adsorption, capillary condensation, molecular simulation

1 INTRODUCTION

Adsorption in nanoporous materials attracts a great deal of attention since it is involved in many industrial processes (catalysis, phase separation, etc.). Adsorption experiments of simple fluids such as argon and nitrogen are also routinely used for the characterization of porous solids: adsorbed amounts and capillary condensation are related to the geometrical properties of the porous matrix [1]. For instance, the specific surface of porous materials is usually assessed from adsorption experiments (prior to the capillary condensation of the fluid) on the basis of the Brunauer, Emmett and Teller (BET) method [1]. The thickness of the film adsorbed on the pore surface t(P) (called t-plot or t-curve) is also an essential parameter to describe the phenomenon of capillary condensation. In the Barrett, Joyner and Halenda (BJH) method, the pore size distribution is estimated from the adsorption isotherm using the Kelvin equation, in which the pore radius R_0 is replaced by the core radius *i.e.* the R_0 - t(P) [1]. From a fundamental viewpoint, studies of gas adsorption in nanopores are aimed at understanding the physics of confined systems. Many theoretical/simulation works for simple pore geometries (slit-shaped and cylindrical pores) have shown that confinement strongly affects the thermodynamic properties of fluids (for a review see [2,3]). However, the effects of the pore morphology (pore shape) and topology (connected or unconnected pores) remain to be clarified.

Comparison of the theoretical predictions with experimental data is often difficult as theories/models are usually developed for structureless pores of a simple geometry. On the other hand, molecular simulations allow studying gas adsorption in realistic pores, provided that atomistic models are available [4,5,6,7,8,9,10]. Molecular simulations are thus an essential tool to link theories developed for simple pore geometries (slit or cylindrical pore) and experimental results obtained for real porous materials. We studied using Grand Canonical Monte Carlo (GCMC) simulations the adsorption of argon at 77 K in silica porous materials of different morphologies/topologies but the same average pore size (3.6 nm). We consider regular cylindrical pores and straight channels having an ellipsoidal section. We also study the adsorption of gas in a cylindrical pore having a constriction, and in a disordered sample of controlled porous glass (Vycor). For the different pore geometries, we discuss the validity of the BET and BJH methods to assess specific surface and pore size distribution from Ar adsorption data.

2 COMPUTATIONAL DETAILS

The Grand Canonical Monte Carlo technique consists of determining the properties of a system having a constant volume V (the pore with the adsorbed phase) in equilibrium with an infinite fictitious reservoir of particles imposing its chemical potential μ and its temperature T. Pores used in our simulations were prepared from a cube of non porous silica cristoballite. This allows cutting out portions of this initial volume in order to obtain different porous matrices. In order to model the pore inner surface in a realistic way, we removed all silicon atoms being in an incomplete tetrahedral environment and all non-bonded oxygen atoms. The electroneutrality of the simulation box is ensured by saturating all oxygen dangling bonds with hydrogen atoms; the partial charges carried by the atoms of the substrate are q_O = -1e, q_{Si} = +2e and q_H = +0.5e. Regular or irregular cylindrical pores can be easily prepared with this procedure: pores are defined by simple mathematical functions. This method has also been used [11] to generate 3D numerical matrices of 'Vycor' glass that account for the morphology and the topology of the real material (see

figure 1). The sample studied in this paper has been obtained by an off-lattice reconstruction method described elsewhere [12,13]. Pellenq and Levitz [5] have calculated the chord length distribution of the numerical Vycor-like sample shown in Figure 1. This exact geometrical pore size distribution exhibits two main peaks (bi-modal distribution d ~ 2.5 and 5.0 nm), corresponding to the average pore size of constricted and bulkier regions, respectively; the mean pore size is 3.6 nm.

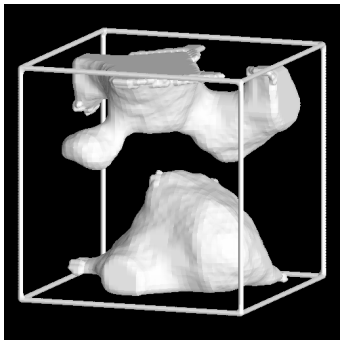

Figure 1: Model of a Vycor sample obtained using an atomistic off-lattice method. The box length is 10.695 nm. One sees through the silica matrix; the porosity is in gray.

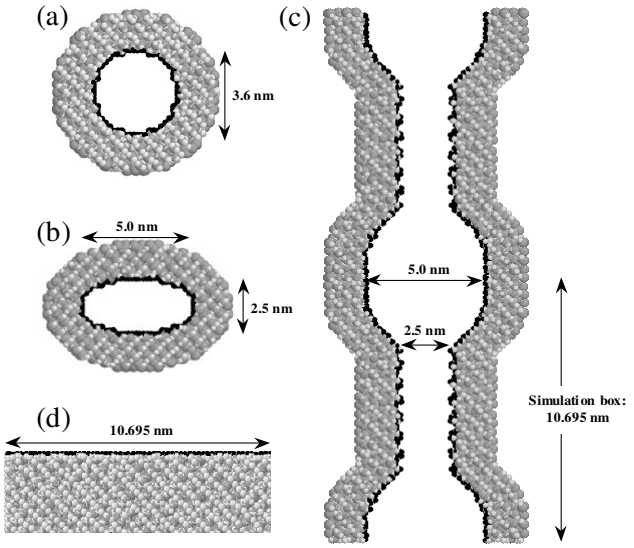

Figure 2: Transversal or plane views of silica nanopores having different shapes: (a) 3.6 nm regular cylindrical pore, (b) 2.5 × 5.0 nm ellipsoidal pore, (c) 5.0 nm cylindrical pore having a 2.5 nm constriction and (d) planar surface. White and gray spheres are respectively oxygen and silicon atoms. Black spheres correspond to hydrogen atoms, which delimit the pore surface.

In this study, we have also considered silica pores of various shapes having the same average pore size, 3.6 nm, as that of the Vycor-like sample. Figure 2 presents the different atomistic silica nanopores that have been prepared for this work. We have generated (see Figure 2a) a cylindrical pore having a pore diameter of 3.6 nm and an infinite length due to periodic boundary conditions applied in the direction of the pore axis (the length of the simulation box is 10.695 nm). We have also prepared (*i*) an ellipsoidal pore having a section of 2.5 nm by 5.0 nm (small and large diameters) and (*ii*) a cylindrical pore with constriction having a largest cavity diameter of 5.0 nm and a constriction diameter of 2.5 nm (see Figure 2b and c). The ellipsoidal and constricted pores also have an infinite length due to periodic boundary conditions applied in the direction of the pore axis. For the ellipsoidal and constricted pores, we define the equivalent regular pore as the cylindrical pore with a circular section (constant along the pore axis) having the same length and volume. Following this definition, both the 2.5 × 5.0 nm ellipsoidal and 2.5-5.0 nm constricted pores correspond to the regular cylindrical pore having a diameter of 3.6 nm. The advantage of comparing these equivalent pores is that it allows the study of adsorption/condensation in pores of various shapes but having the same average 'confinement'. In addition, the bi-modal size distribution for the ellipsoidal pore and the constricted pore (2.5 and 5.0 nm) are identical to that obtained for the Vycor-like' sample. Finally, we have also simulated the adsorption of Ar atoms on a plane substrate in order to determine reference data for the thickness of the adsorbed film (the plane surface having a square section of 10.695 × 10.695 nm is shown in Figure 2d).

3 RESULTS AND DISCUSSION

Figure 3 shows the Ar adsorption isotherms at 77 K for the 3.6 nm cylindrical pore, the 2.5 × 5.0 nm ellipsoidal pore and the 2.5-5.0 nm constricted pore. The condensation pressure for the ellipsoidal pore ($P \sim 0.10\ P_0$) is lower than that for the cylindrical pore ($P \sim 0.14\ P_0$). This shows that the morphologically disordered pore shape in the case of the ellipsoidal geometry affects the condensation pressure. Malanoski and Van Swol have obtained a similar result for a rectangular pore using lattice density functional theory [14]. We note that the condensation/evaporation mechanisms are the same as those obtained for the regular cylindrical nanopore. The condensation pressure for the 2.5 × 5.0 nm ellipsoidal is also smaller than that for the 2.5 nm cylindrical part of the constricted pore $P \sim 0.04\ P_0$ (see figure 5b). The desorption pressure for the ellipsoidal pore, $P \sim 0.07\ P_0$, is lower than that for the cylindrical pore, $P \sim 0.09\ P_0$, (both evaporation processes correspond to the nucleation of a gas bubble since there is no interface between the confined liquid and the gas reservoir). This result suggests that the emptying process through cavitation is driven by the smallest size of the pore. These results are in full agreement with our previous study [9]. However, recent simulation results by Sarkisov and Monson [15] have shown that the desorption in a constricted slit pore is rather controlled by the size of the cavity than that of the constriction.

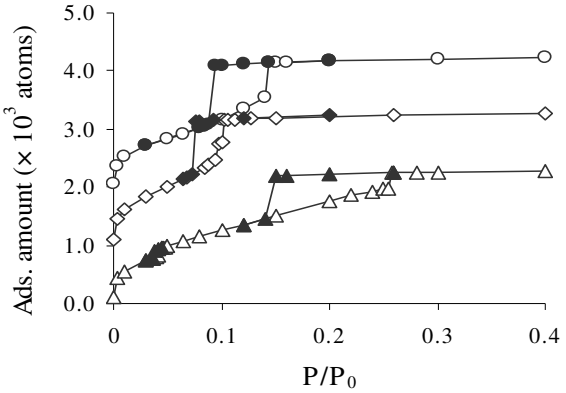

Figure 3: Ar adsorption isotherm at 77 K in silica pores of various morphologies: (circles) cylindrical pore 3.6 nm, (diamonds) ellipsoidal pore 2.5 × 5.0 nm and (triangles) 5.0 nm cylindrical pore with a 2.5 nm constriction. Open and closed symbols correspond to adsorption and desorption processes, respectively. For sake of clarity, the adsorption isotherms for the cylindrical and ellipsoidal pores have been shifted up by +2.0 and +1.0, respectively.

We now discuss the results for the pore with the constriction. At low pressures, the pore surface is covered by a quasi-homogeneous layer of Ar atoms. The filling of the pore with constriction starts at P = 0.04 P_0 with the condensation of Ar atoms in the 2.5 nm cylindrical part of the constricted pore. As expected, this condensation pressure is smaller than that obtained for the 3.6 nm cylindrical pore. The condensation in the constricted part leads to the presence of hemispherical menisci in the interfacial region between the largest cavity and the constriction. These curved interfaces together with the film adsorbed on the wall of the 5.0 nm cavity define a gas bubble inside the pore. As the pressure increases, we observe the displacement at equilibrium (reversible) of these menisci towards the center of the 5.0 nm cavity, *i.e.* the radius of the gas bubble located inside the pore diminishes. Finally, the pore gets completely filled once the condensation of the gas bubble occurs at a pressure P ~ 0.26 P_0. Due to the different condensation pressures for the 2.5 nm constriction and 5.0 nm cavity, the adsorption branch for the constricted pore appears much smoother than that observed for the 3.6 nm regular pore. Starting with the completely filled pore, the desorption branch for the constricted pore is a two-step process. As the pressure decreases, we first observe desorption of Ar atoms confined in the 5.0 nm part of the pore. Due to the infinite length of the pore, this evaporation mechanism is necessarily a metastable transition involving a cavitation phenomenon. The desorption of Ar atoms confined in the 5.0 nm cavity occurs at P ~ 0.15 P_0 which is much higher than that for the ellipsoidal pore (P ~ 0.07 P_0) and that for the 3.6 nm cylindrical pore (P ~ 0.09 P_0). This result supports the previous conclusion that the 'cavitation' pressure decreases as the cavity size decreases. Finally, the desorption mechanism ends with the desorption at P ~ 0.038 P_0 of Ar atoms in the 2.5 nm constriction region.

We now discuss the validity of the BET method [1] to assess specific surface from adsorption data in porous materials having different morphologies and topologies. A comparison between the BET surface and the geometrical surface is reported in table 1 for each pore geometry. We have also reported the result for the Vycor-like matrix that has been previously discussed by Pellenq *et al.* [16]. The monolayer capacity has been converted into a surface area using the common value for atomic surface area for an Ar atom at 77 K a(Ar) = 0.138 nm^2 [1]. One can see in table 1 that, for the plane substrate (the most simple system) the BET surface is much larger (25 %) than the true surface. We note that Gelb and Gubbins [4], in their simulation study of nitrogen adsorption at 77 K on a planar substrate, found that the BET surface is in good agreement with the geometrical surface. This shows that the specific surface assessed from adsorption data depends strongly on the choice of the adsorbate. In the case of the 3.6 nm cylindrical pore, our simulations show that the disagreement between the BET surface and the geometrical surface (49 %) is increased compared to the plane surface. This shows that the effect of confinement is to increase the overestimation by the BET method of the pore surface. Gelb and Gubbins [4] reached a similar conclusion; showing that the confinement leads to an increase in the density of the first monolayer adsorbed on the pore wall (due to a larger fluid/substrate interaction for a cylindrical pore compared to a planar substrate). This may explain why the ratio between the BET surface and the geometrical surface in our study is larger for the cylindrical pore than that for the plane substrate, since we kept the monolayer density, a(Ar) = 0.138 nm^2, constant in our calculations of the BET surface. The effect of the distorted shape of the pore on the surface assessed by the BET plot can be estimated by comparing results in table 1 for the cylindrical pore and the ellipsoidal pore (since those pores have the same average pore size 3.6 nm *i.e.* the same confinement). We have found that the ratio of the BET surface to the geometrical surface is 1.81 for the 2.5 × 5.0 nm ellipsoidal pore. This indicates that the high curvature regions of the ellipsoidal section increases the discrepancy between the BET surface and the geometrical surface. Interestingly, we observe that the ratio of the BET surface to the geometrical surface for the constricted pore (1.27) is much smaller than that for the ellipsoidal pore and even smaller than that for the regular cylindrical pore. It seems that, in the case of the constricted pore, the BET surface is much closer to the geometrical surface due to the negative curvatures offered by this pore geometry (at the interfacial region between the constriction and the cavity parts). Thus, these negative curvature regions may compensate (more or less) the positive curvature regions of the cylindrical parts. This idea

is supported by results obtained for the Vycor-like sample that exhibits a non-regular surface with many mesoporous regions of negative curvature: for this fully disordered porous matrix, the BET surface underestimates (by 29 %) the geometrical surface, in contrast to the other pore geometries that exhibits no topological disorder.

Substrate	Planar	Cylinder (3.6nm)	Ellipse	Constricted pore	Vycor
S_{BET}/S_{GEO}	1.25 (7)	1.49 (6)	1.81 (6)	1.27 (6)	0.71 (6)

Table 1: Comparison for different substrates between the BET surface assessed and the 'true' geometrical surface. The number in parentheses indicates the relative error (%).

We now discuss the validity of the BJH method to extract a pore size distribution from Ar adsorption isotherms at 77 K. We have analyzed the adsorption branch of the Ar isotherm for the different pore geometries studied in this work. Table 2 shows the pore diameter assessed using the BJH method for the regular cylindrical pore, the ellipsoidal pore and the constricted pore. The BJH method largely underestimates the diameter of the 3.6 nm cylindrical pore. In the case of the ellipsoidal pore, the pore diameter assessed using the BJH method (d ~ 0.62 nm) is also significantly lower than both the large and small dimensions of the pore (d ~ 2.5 and 5.0 nm). Furthermore, one can see that the disagreement between the BJH diameter and the true diameter is larger for the ellipsoidal pore than that for the cylindrical pore. This shows that the morphological disorder for the ellipsoidal geometry increases the underestimation by the BJH method of the pore diameter. We now consider the case of the 2.5 nm and 5.0 nm parts of the constricted pore. As in the case of the 3.6 nm cylindrical pore, the BJH method also underestimates the diameter of the constricted region. In addition, one can see that for these two cylindrical pores, the disagreement between the BJH pore diameter and the geometrical pore diameter becomes larger as the pore size decreases. This idea is supported by the fact that in the case of the largest cavity (5.0 nm) of the constricted pore the BJH method leads to a pore diameter closer to the geometrical size than for the other pores.

We have also analyzed Ar adsorption data for the Vycor sample using the BJH method. The pore size distribution extracted using the BJH analysis has a very different shape from that of the chord distribution. However, the BJH pore size distribution has two peaks as in the case of the chord distribution. These peaks are shifted towards the smaller pore-size domain by roughly 1 nm in agreement with recent simulation results on similar materials [17]. Interestingly, the most marked peak obtained with the BJH analysis corresponds to the mean value of the chord distribution (d = 3.6 nm).

Substrate	Cylinder 3.6nm	Ellipse	Constricted pore 2.5 nm part	Constricted pore 5.0 nm part*
P/P_0 cond.	0.142	0.101	0.043	0.255
$t(P/P_0)$ (nm)	0.38	0.33	0.27	0.50
D (nm)	0.73	0.62	0.47	1.43

Table 2: BJH pore size for porous substrates with various morphologies. The pore size has been determined from the adsorption branch of the Ar adsorption.

REFERENCES

[1] F. Rouquerol, J. Rouquerol, and K. S. W. Sing, *Adsorption by Powders and Porous Solids*, Academic Press: London, 1999.

[2] L. D. Gelb, K. E. Gubbins, R. Radhakrishnan and M. Sliwinska-Bartkowiak, Rev. Prog. Phys. 62, 1573, 1999.

[3] C. Alba-Simionesco, B. Coasne, G. Dosseh, G. Dudziak, K. E. Gubbins, R. Radhakrishnan and M. Sliwinska-Bartkowiak, J. Phys.: Condens. Matter 18, R15 (2006).

[4] L. D. Gelb and K. E. Gubbins, Langmuir 14, 2097, 1998.

[5] R. J. M. Pellenq and P. E. Levitz, Mol. Phys. 100, 2059, 2002.

[6] K. S. Page and P. A. Monson, Phys. Rev. E 54, 6557, 1996.

[7] J. Pikunic, C. Clinard, N. Cohaut, K. E. Gubbins, J. M. Guet, R. J. M. Pellenq, I. Rannou and J. N. Rouzaud, Langmuir 19, 8565, 2003.

[8] B. Coasne and R. J. M. Pellenq, J. Chem. Phys. 120, 2913, 2004.

[9] B. Coasne and R. J. M. Pellenq, J. Chem. Phys. 121, 3767, 2004.

[10] B. Coasne, K. E. Gubbins and R. J. M. Pellenq, Part. Part. Syst. Charact. 21, 149, 2004.

[11] R. J. M. Pellenq, B. Rousseau, and P. E. Levitz, Phys. Chem. Chem. Phys. 3, 1207, 2001.

[12] P. E. Levitz, Adv. Coll. Interface Sci. 76-77, 71, 1998.

[13] R. J. -M. Pellenq, A. Delville, H. Van Damme, and P. E. Levitz, Studies in Surface Science and Catalysis Vol. 128, Elsevier Science, page 1, 2000.

[14] A. P. Malanoski and F. Van Swol, Phys. Rev. E 66, 041602, 2002.

[15] L. Sarkisov and P. A. Monson, Langmuir 17, 1600, 2001.

[16] R. J. M. Pellenq, S. Rodts and P. E. Levitz, Mat. Res. Soc. Symp. Proc. 651, 2001.

[17] L. D. Gelb and K. E. Gubbins, Langmuir 15, 305, 1999.